metals

MDPI

Article

Precipitation Behavior and Strengthening–Toughening Mechanism of Nb Micro-Alloyed Direct-Quenched and Tempered 1000 MPa Grade High-Strength Hydropower Steel

Zhongde Pan [1,2,†], Enmao Wang [1,†] and Huibin Wu [1,*]

[1] Collaborative Innovation Center of Steel Technology, University of Science and Technology Beijing, Beijing 100083, China
[2] Nanjing Iron and Steel Co., Ltd., Nanjing 210035, China
* Correspondence: whbustb@163.com
† These authors contributed equally to this work.

Abstract: Faced with the rapid development of large-scale pumped-storage power stations, the trade-off between the strength and toughness of hydropower steels in extreme environments has been limiting their application. The effects of Nb micro-alloying and direct quenching and tempering processes on the strengthening–toughening mechanism of 1000 MPa grade high-strength hydropower steel are studied in this paper, and the precipitation behavior of Nb is discussed. The results showed that only the 0.025Nb steel using the DQT process achieved a cryogenic impact energy of more than 100 J at −60 °C. Under the DQT process, a large number of deformation bands and dislocations were retained, refining the prior austenite grains and providing more nucleation sites for the precipitation of NbC during the cooling process. The DQT process has a more obvious local strain concentration, mainly focusing on the refined lath boundary, which indicates that the refinement of the microstructure also promotes the stacking of dislocations. The improvement in fine grain strengthening and dislocation strengthening by the DQT process jointly led to an increase in strength, resulting in a better combination of strength and toughness.

Keywords: Nb micro-alloying; hydropower steel; precipitation; strengthening–toughening

check for updates

Citation: Pan, Z.; Wang, E.; Wu, H. Precipitation Behavior and Strengthening–Toughening Mechanism of Nb Micro-Alloyed Direct-Quenched and Tempered 1000 MPa Grade High-Strength Hydropower Steel. *Metals* **2024**, *14*, 794. https://doi.org/10.3390/met14070794

Academic Editors: Hardy Mohrbacher, Chongze Hu and Xin Wang

Received: 15 May 2024
Revised: 2 July 2024
Accepted: 5 July 2024
Published: 8 July 2024

Copyright: © 2024 by the authors. Licensee MDPI, Basel, Switzerland. This article is an open access article distributed under the terms and conditions of the Creative Commons Attribution (CC BY) license (https://creativecommons.org/licenses/by/4.0/).

1. Introduction

The global energy pattern has undergone significant changes and is transforming to clean and renewable energy, involving the most crucial issue of power system selection [1,2]. The growing popularity of solar and wind as clean energy sources has effectively reduced dependence on fossil fuels, but their intermittent nature makes it difficult to provide a stable and continuous power supply [3]. However, pumped storage has become an excellent solution to support grid-connected renewable energies by utilizing water as a medium to achieve large-scale reversible energy storage and power supply through the simple inter-conversion of electrical energy and potential energy [4,5]. In the face of the rapid development of hydropower and large-scale pumped-storage power stations, designing steel with high strength and toughness for hydropower has become a top priority. This is to meet the requirements of higher water pressure and larger pipe diameter, to reduce the weight of the structure and improve safety [6]. Therefore, it is necessary to choose the appropriate chemical composition and process to break through the limitation of the trade-off between the strength and toughness of steel on application. In addition, excellent weldability should be taken into account, while achieving the perfect combination of strength and toughness [7–9].

As an energy-saving technology, the direct quenching-after-rolling (DQT) process has been gradually applied to the production of high-strength low-alloyed (HSLA) steel with the development of the controlled cooling process, which can significantly improve the

production efficiency. Moreover, it is well suited for the development background of clean energy [10,11]. Compared to the conventional reheating, quenching and tempering (QT) process, the low final rolling temperature of direct quenching, coupled with the subsequent rapid cooling can combine the high density of dislocations due to deformation energy storage with a fine microstructure, resulting in a balance of strength and toughness not achievable with the QT process [12]. The strength advantage of steels after direct quenching is mainly reflected in high dislocation strengthening and high precipitation strengthening, while the toughness is generally determined by the fineness of the microstructure and high energy interfaces (e.g., high-angle grain boundaries, HAGBs) to resist fracture [13,14]. In recent years, the concept of quenching and partitioning (Q & P) has been widely accepted as a potential process for adjusting the balance between the elongation at break and tensile strength of advanced high-strength steels [15,16]. Recently, Ghosh et al. [17] have explored the new processing concept of direct quenching and partitioning (DQP) using medium carbon steel, resulting in a fine acicular aggregate of carbon-depleted, highly refined martensitic nano-laths, with fine retained austenite (RA) films. Most of the highly stable austenite is retained due to effective partitioning, even at low partitioning temperatures. The DQP process promotes the fine splitting of the prior austenite grain (PAG) packages and RA films, contributing to a favorable combination of mechanical properties, including a high yield strength of 1000~1200 MPa, a tensile strength of 2100~2300 MPa and moderate impact toughness transition temperature T_{28J} of −5~12 °C. In addition, Wu et al. [18] have prepared X80 pipeline steel by the DQT process and focused on the effects of finish rolling temperature and tempering temperature on the microstructure and mechanical properties. It was shown that the granular bainite in the quenched microstructure is beneficial to the formation of fine polygonal ferrite in the tempered microstructure, and the precipitation characteristics of the pre-existing TiC particles promote the generation of finely dispersed precipitates in the subsequent tempering, while achieving an ideal combination of yield strength (~632 MPa), tensile strength (~707 MPa) and impact energy (~249 J at −20 °C).

The microstructure evolution of medium- and low-carbon martensitic steels and bainitic steels obtained by the traditional QT process is weakly affected by chemical composition. It is generally believed that it mainly depends on the stress relaxation of tempering to improve the toughness [19]. However, the effect of tempering on the toughness of directly quenched steels is complex. Moreover, it is crucial to exert the structural heritability in contributing to the precipitation behavior of directly quenched steels with different chemical composition during tempering [20]. The strong interaction dislocations between nano-scale precipitates play an important role in strengthening HSLA steels, with the accompanying fine-grain strengthening and precipitation strengthening minimizing the loss of strength due to the decrease in the carbon content and consequent reduction in solid solution strengthening [21,22]. Previous studies have shown that Nb plays a role in solute drag and precipitation pinning effects, with dislocation climbing to delay austenite recrystallization at high temperatures [23,24]. Its beneficial effect on low-temperature controlled rolling is higher than that of V and Ti. Recently, Tian et al. [25] have revealed that replacing part of V with Nb in high-carbon (~0.77 wt%) pearlite steels compensated for toughness by introducing more HAGBs and a more uniform grain size distribution, which is conducive to obtaining the finest microstructure and the optimal comprehensive mechanical properties. Bai et al. [26] have also shown that Nb-bearing steels exhibit the optimal toughness for low carbon pipeline steels, followed by Nb-Mo steels and finally Ti-Mo steels. The nano-precipitates of Nb refine the austenite grains by hindering grain boundary migration and provide favorable nucleation sites for phase transformation, thereby enhancing the strength and toughness. However, few studies have focused on the role of Nb in DQT steels, especially the difference in tempering precipitation behavior and strengthening–toughening, compared to the traditional QT process.

This paper aims to develop a new generation of low-carbon niobium micro-alloyed 1000 MPa grade high-strength hydropower steel by using the Nb microalloying design and direct quenching process. The content of C and P_{cm} was further reduced, and the reduction

of Cr, Mo, Ni and other alloys was realized. The effects of Nb addition on the mechanical properties and microstructure of the steels after conventional QT and DQT, respectively, were analyzed comparatively. The precipitation behavior of Nb and its mechanism for the enhancement of strength and toughness of 1000 MPa high-strength hydropower steel were discussed in detail.

2. Materials and Methods

The chemical composition of the steels prepared in this study is shown in Table 1. The slabs were smelted and produced by Nanjing Iron and Steel Group (Nanjing, China), based on the Nangang wide plate production line. The billets were heated to 1200 °C and held for 2 h, and then controlled rolling was carried out in two stages. The first stage was rolled in the recrystallization zone greater than 1000 °C, and the second stage was rolled with the final rolling temperature of ~850 °C. The plates were rolled to a thickness of 48 mm. Subsequently, direct quenching + tempering (DQT) and off-line quenching + tempering (QT) were employed, respectively, and the steels, after off-line quenching, were reheated to 900 °C for austenization. To analyze the effect of Nb addition on the microstructure and mechanical properties of the DQT steels and QT steels, the tempering was set at 550 °C for 40 min. On this basis, the steels were then tempered at 450 °C and 650 °C, respectively, to fully discuss the effect of quenched microstructure on the precipitation behavior of Nb at different tempering temperatures. The schematic diagrams of the heat treatment processes are shown in Figure 1.

Table 1. The chemical composition of the prepared hydropower steels (wt.%).

Steel	C	Mn	Si	Alt	Nb	V	Ti	Cr	Ni	Mo	P_{cm}
0Nb	0.10	1.05	0.21	0.041	-	0.046	0.015	0.35	0.30	0.39	0.21
0.025Nb	0.08	1.06	0.19	0.036	0.025	0.043	0.012	0.32	0.28	0.41	0.19

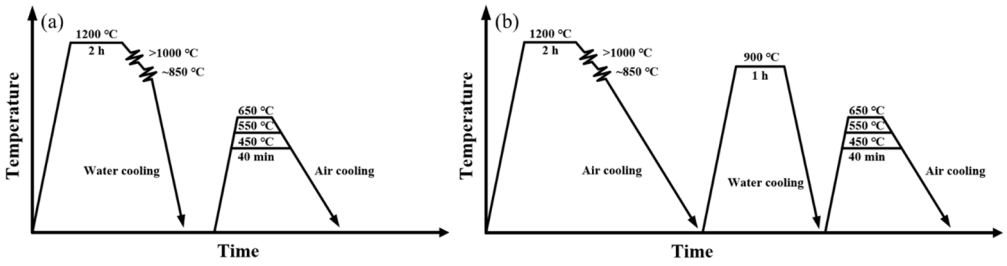


Figure 1. Schematic diagrams of (**a**) DQT and (**b**) QT processes.

According to the standard of ASTM E8 [27], the tensile tests were conducted on a CMT5386 electronic universal testing machine (New Sansi Laboratory Equipment Co., LTD., Shenzhen, China), with a tensile rate of 2×10^{-3} s^{-1} and a test direction of the rolling direction. The tensile samples were machined with a gauge length of 25 mm and a thickness of 2 mm. The cryogenic impact tests at −60 °C were conducted on a JBDW-300D ultra-low temperature impact testing machine (Koohei Test Machine Co., Ltd., Jinan, China), with a sample size of $10 \times 10 \times 55$ mm^3. Three parallel samples were taken at 1/4 of each steel plate for both tensile and cryogenic impact tests.

Metallographic samples with dimensions of 6 mm × 4 mm × 3 mm were cut along the rolling direction at 1/4 of each steel plate by wire cutting and polished using sandpaper grits from 240 up to 2000 in sequence, followed by 0.25 μm diamond polishing paste and mechanically polished until the surface was mirror-like, respectively. The microstructure was observed under a COSSIM optical microscope (OM, Beijing Century Science and Technology Instrument Co., Ltd., Beijing, China) by etching with 4% nital, and the microstructure was observed under a ZEISS ULTRA 55 field emission scanning electron microscope (SEM, Carl Zeiss AG, Oberkochen, GER) with an operating voltage of 5 kV. The

samples were electrolytically polished with 3% HF + 28% H_2O_2 + 69% H_2O solution at a voltage of 20 V, a current of 1 A, and an electrolytic polishing time of 20 s. The XRD tests were performed at a scanning rate of 1°/min with a step size of 0.02, and the dislocation density was calculated by the following formula [28,29]:

$$\rho = 14.4\frac{e^2}{b^2} \quad (1)$$

where e represents the microstrain due to grain size and strain calculated using Jade 6.0 software, and b is the Burgers vector (0.248 nm). The samples were observed and analyzed for grain orientation, the angular distribution of grain boundaries and microscopic strain distribution using the EBSD probe and AztecCrystal analysis software (Version 2.1) in a ZEISS GeminiSEM500 field emission scanning electron microscope (Carl Zeiss AG, Oberkochen, Germany) with a scanning voltage of 20 kV and a step size of 0.12 μm. The samples were cut into 1 mm slices by a wire cutter and polished to a thickness of 50 μm with sandpapers, followed by double-jet thinning to 30 μm circular slices to observe the microstructure and dislocation configuration under an FEI Talos F200X transmission electron microscope (TEM, FEI Company, Hillsborough, OR, USA). The samples of the precipitates were prepared by extraction-replica: the samples were etched with 3% nital, followed by surface spray-plating with a carbon film and stripping of the film with 5% nital. Finally, after being washed with alcohol and deionized water, they were picked up with a 150-mesh copper mesh.

3. Results and Discussion

3.1. Mechanical Properties

The engineering stress–strain curves and tensile properties of the prepared hydropower steels are shown in Figure 2a,b. Due to the combined effect of solid solution strengthening and precipitation strengthening of Nb, the yield strength of 0.025Nb steel after DQT reaches the highest value of 986 MPa, the tensile strength is as high as 1037 MPa, and the elongation after fracture is still 17.5%. The addition of 0.025%Nb resulted in the optimum tensile properties of the steel.

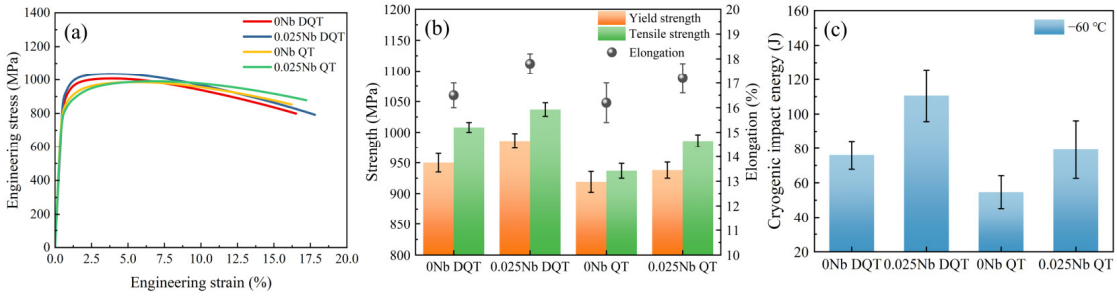


Figure 2. (**a**) Engineering stress–strain curves, (**b**) tensile properties and (**c**) cryogenic impact toughness of the prepared steels.

Although the QT process can still realize the production of 1000 MPa grade hydropower steel, by contrast, DQT can further improve the strength and ductility while saving the process cost. The cryogenic impact energy of the prepared steels at −60 °C is shown in Figure 2b. For the 0Nb steel, the cryogenic impact toughness at −60 °C is poor, and the cryogenic toughness under the DQT process is better than that under the QT process. After adding 0.025%Nb, the cryogenic impact energy at −60 °C can increase to ~110 J using the DQT process. Combined with the tensile properties, it was further found that the cryogenic impact toughness of 0.025Nb steel is significantly improved, and it still has the optimum strength–ductility matching. Therefore, it is necessary to add the appropriate content of Nb to ensure the cryogenic impact toughness for the production of 1000 MPa grade hydropower steel.

3.2. Microstructure

The DQT and QT treatments were performed on 0Nb steel and 0.025Nb steel, respectively. The tempering temperature was 550 °C, and the SEM micrographs are shown in Figure 3. It can be seen from Figure 3a,b that there are obvious deformation microstructure characteristics of the two steels after DQT, and the prior austenite grains are elongated along the rolling direction, indicating that the lower finishing-rolling temperature and larger pass reduction are adopted in the rolling process, and the direct quenching retains this deformation microstructure characteristics. After tempering, the sub-boundaries in the steels became blurred, and the martensite laths recovered with a large number of precipitated cementite particles and carbide particles. Nb is a strong carbonitride-forming element that can form carbides and nitrides with high melting points and high hardness [30]. It can play two roles in steel. First, because the precipitates have a high melting point and precipitate on the austenitic grain boundaries, their solid solubility at high temperatures is low, which can prevent the growth of austenitic grains, thereby greatly refining the grains [31]. The second is that Nb dissolved in austenite will precipitate during the transformation process of austenite, which will hinder the movement of dislocations in the lattice of iron atoms, further improving the strength [32]. Therefore, compared to 0Nb steel, the grain size and precipitate size of 0.025Nb steel are significantly refined. In addition to the cementite particles, there are also a large number of Nb precipitates, which will be discussed in detail in Section 3.4. The combined effect of fine-grain strengthening and precipitation strengthening increased the yield strength and tensile strength of 0.025Nb steel by about 36 MPa, and the Nb precipitates had no adverse impact on ductility. From the results of cryogenic impact energy at −60 °C, it can be seen that the grain refining effect brought about by the addition of Nb not only further improves the strength, but also increases the barrier effect on crack growth, resulting in a significant improvement in low-temperature impact toughness. The 0.025Nb steel reached a cryogenic impact energy over 100 J at −60 °C, achieving excellent strength–toughness matching. Figure 3c,d show that the microstructure of the QT-treated 0.025Nb steel is also somewhat refined compared to that of the 0Nb steel, but not as pronounced as that obtained after the DQT process.

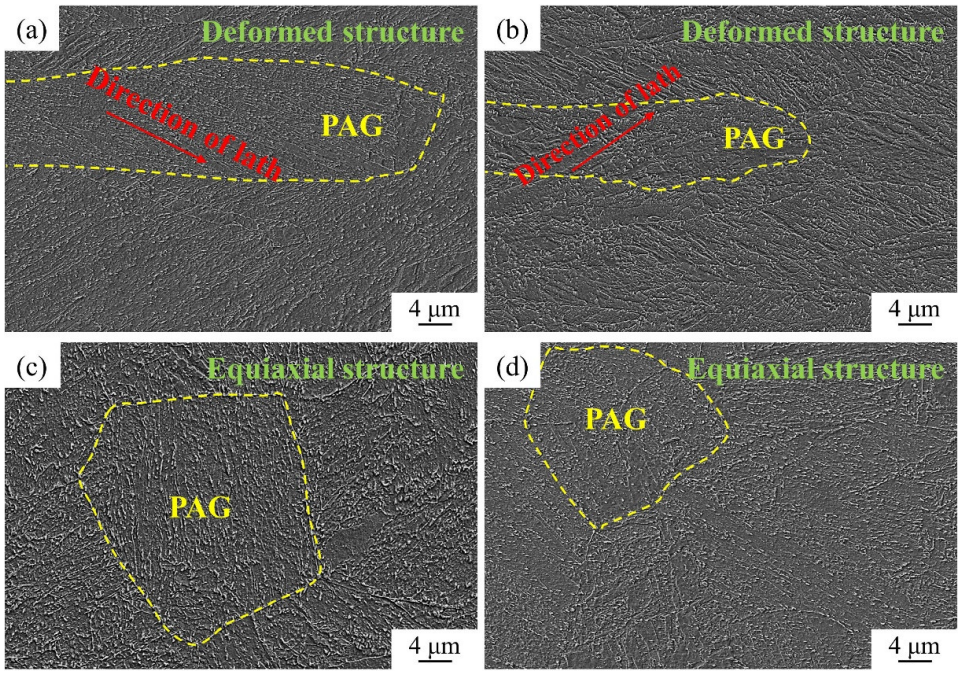


Figure 3. SEM micrographs of the prepared steels after different heat treatment processes. (**a**) 0Nb DQT, (**b**) 0.025Nb DQT, (**c**) 0Nb QT, (**d**) 0.025Nb QT.

Figure 4 shows the XRD patterns and quantitative results of the dislocation density. Direct quenching retained a large number of deformed dislocations in the deformed austenite grains, and the entanglement of dislocations hindered the growth of the martensite laths [33]. Therefore, the direct quenching structure had a higher density of dislocations (0Nb DQT: 1.2×10^{15} m^{-2}, 0.025Nb DQT: 1.8×10^{15} m^{-2}), a higher number of substructures and finer martensite laths (~219 nm). During quenching, a large number of deformation bands, dislocations and other defects existed within this austenite grain, dividing the prior austenite grain, increasing the effective grain boundary area and providing more nucleation locations for the phase transformation, resulting in a finer microstructure [34]. In the deformed austenite grain, the martensite laths grew along a certain angle to the austenite grain boundary until they met another austenite grain boundary in the growth direction, forming a lath that ran through the entire austenite grain. After accumulated deformation in the non-recrystallized zone, the austenite grains were elongated along the rolling direction. After rolling, most of the austenite grain boundaries were distributed nearly parallel to the rolling direction, which also reduced the effective size of the austenite grains. Therefore, most nucleation and growth of martensite occurred at grain boundaries parallel to the rolling direction, and when the martensite encountered adjacent parallel grain boundaries, its growth stopped. The DQT process can ensure high strength and achieve excellent strength–ductility–toughness matching by refining the grains.

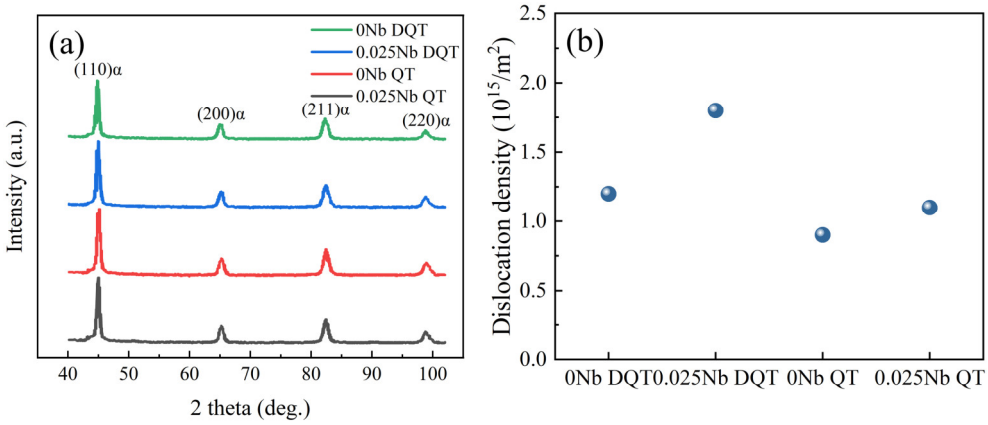


Figure 4. (**a**) XRD patterns and (**b**) dislocation density of the prepared steels after different heat treatment processes.

The austenitizing process was repeated during offline quenching, and the austenite grain was fully grown. After quenching, the prior austenite grain size was retained, which also made the martensite laths (~293 nm) wider after quenching, and the structure coarsened after tempering. Generally speaking, the QT process of offline quenching can improve toughness by increasing the tempering temperature [35]. However, for medium-thick plates with larger thicknesses, there is a temperature gradient along the thickness direction during tempering. The tempering temperature too close to A_{c1}, followed by the subsequent air-cooling with reddening of the center towards near the surface, has a probability of making the temperature near the surface higher than A_{c1}, resulting in partial austenitization. After cooling, there are M/A islands of different sizes distributed along the prior austenite grain boundaries. The interface between the soft-phase ferrite and a certain size of the hard-phase M/A island is prone to become the location of crack nucleation [36]. Combined with the occurrence of high-temperature temper brittleness, the QT process is not conducive to the improvement in strength and toughness of hydropower steel.

3.3. Fracture Morphology and Strengthening–Toughing Mechanism

3.3.1. Impact Fracture Morphology

Comparing the strength and impact properties of 0.025Nb steel under the DQT and QT processes, it can be seen that the direct quenching of DQT not only improves the strength, but also greatly improves the toughness, which is generally higher than that of the QT process. This is because of the former fully preserved deformation dislocations, which were mostly pinned by NbC, resulting in poor mobility and, in turn, promoting the increase in strength. However, the orientation difference between the martensite laths in the subgrain is large, which had a certain effect on the propagation of micro-cracks, thereby improving the toughness of the steel [37]. During the tempering of both processes, dispersed and fine NbC precipitates existed. When cracks propagated within the grain, it was difficult to strictly follow a certain crystallographic plane, which was conducive to preventing the formation and propagation of cracks. Figure 5 shows the impact fracture micrographs under the DQT and QT processes. Comparing the fracture morphology of the initial quenched state of the two processes, the fracture morphology after direct quenching is dominated by dimples, and the size and depth of the dimples are unevenly distributed, indicating a ductile fracture (Figure 5a). The fracture morphology after offline quenching is dominated by river-like cleavage steps, characteristic of a typical brittle fracture (Figure 5c). After tempering at 550 °C, the fracture morphology of DQT and QT are both dimples. At this time, the dimples after DQT are deep and uniform in size, belonging to a typical ductile fracture (Figure 5b). After the QT process, the dimples of the fracture surface are uneven and shallow, and there are also some river-like cleavage fracture zones on the fracture surface (Figure 5d). Layered tear edges can be observed along the thickness direction, belonging to a ductile–brittle mixed fracture (Figure 5e).

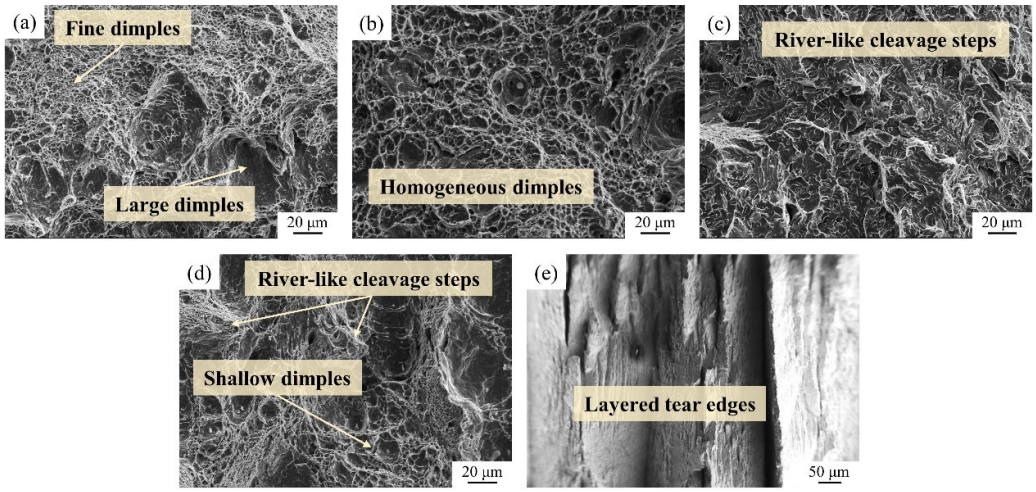


Figure 5. Impact fracture micrographs of 0.025Nb steel under different processes. (**a**) DQT as-quenched, (**b**) DQT tempering at 550 °C, (**c**) QT as-quenched, (**d**,**e**) QT tempering at 550 °C.

3.3.2. EBSD Analysis of the Strengthening–Toughening Mechanism

Figure 6 shows the grain boundary distributions and inverse pole figures (IPF) of 0.025Nb steel subjected to DQT and QT processes, respectively. The red lines represent HAGBs (the orientation difference between adjacent grains is greater than 15°), and the green lines represent low-angle grain boundaries LAGBs (the orientation difference between adjacent grains is 2°~15°), as shown in Figure 6a,b. It can be seen that compared with the QT process, the DQT process significantly refined the martensite laths, and the obvious lath structure can still be observed after tempering. Figure 7a,b show the distribution of grain sizes under two processes. The mean values of effective grain size under the DQT and QT processes are 7.6 μm and 11.1 μm, respectively. The refining effect of the DQT process on martensite blocks and martensite laths can simultaneously improve the yield

strength and impact toughness. It is well known that the cryogenic impact toughness is mainly related to the proportion of HAGBs [38]. As can be seen from Figure 7c,d, the proportion of HAGBs under the DQT and QT processes is 63.6% and 43.2%, respectively. It can be seen that the refining effect of the DQT process on grains significantly increases the proportion of high angle grain boundaries, which can effectively hinder crack growth and promote crack deflection as high-energy interfaces. On the other hand, from the IPF orientation distributions, it can be observed that within a single prior austenite grain, the number and orientation of martensite block units increase under the DQT process, which means that the selectivity of martensite variants increased during transformation [39]. In general, the PAGBs, the packet interface and the block interface of martensite correspond to HAGBs, while the martensite laths are mainly LAGBs, or even a finer substructure unit [40]. Therefore, the improvement in toughness mainly depends on the refinement of prior austenite grains and the refinement of the martensitic block and packet units. The DQT process has achieved the refinement of various structural units well, thereby promoting a significant improvement in cryogenic impact toughness.

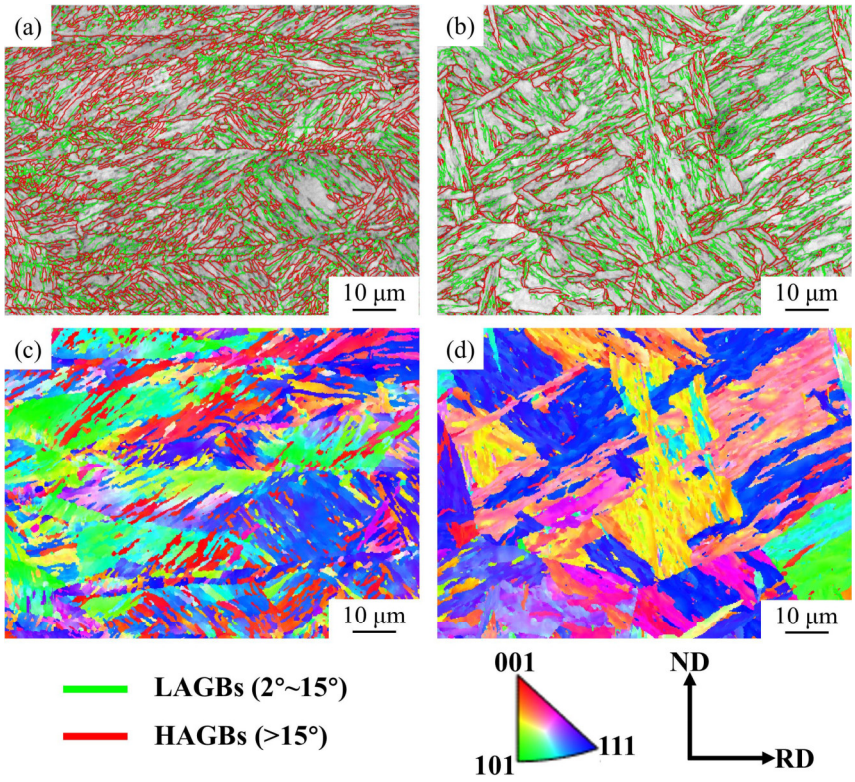


Figure 6. EBSD micrographs of 0.025Nb steel under DQT and QT processes. Grain boundary distributions: (**a**) DQT, (**b**) QT; IPF: (**c**) DQT, (**d**) QT.

In addition to fine grain strengthening and precipitation strengthening, dislocation strengthening is also the main strengthening mechanism for HSLA steels. Figure 8a,b show the kernel average misorientation (KAM) under two processes. It is obvious from the figure that the DQT process has a more obvious strain concentration, mainly focusing on the refined laths boundaries, which indicates that the refinement of the microstructure also promotes the stacking of dislocations. The average KAM values for the two processes are 0.65° and 0.58°, respectively, as shown in Figure 8c,d. By introducing them into the following formula, the geometrically necessary dislocation density can be calculated (ρ_{GND}) [41]:

$$\rho_{GND} = \frac{2KAM_{av}}{ub} \quad (2)$$

where u represents the scanning step size (0.12 μm), and b is the Burgers vector (0.248 nm). According to the above formula, the ρ_{GND} under the DQT and QT processes is 9.3×10^{14} m^{-2} and 8.3×10^{14} m^{-2}, respectively. The improvement in fine grain strengthening and dislocation strengthening by the DQT process has jointly led to an increase in strength, resulting in a better combination of strength and toughness.

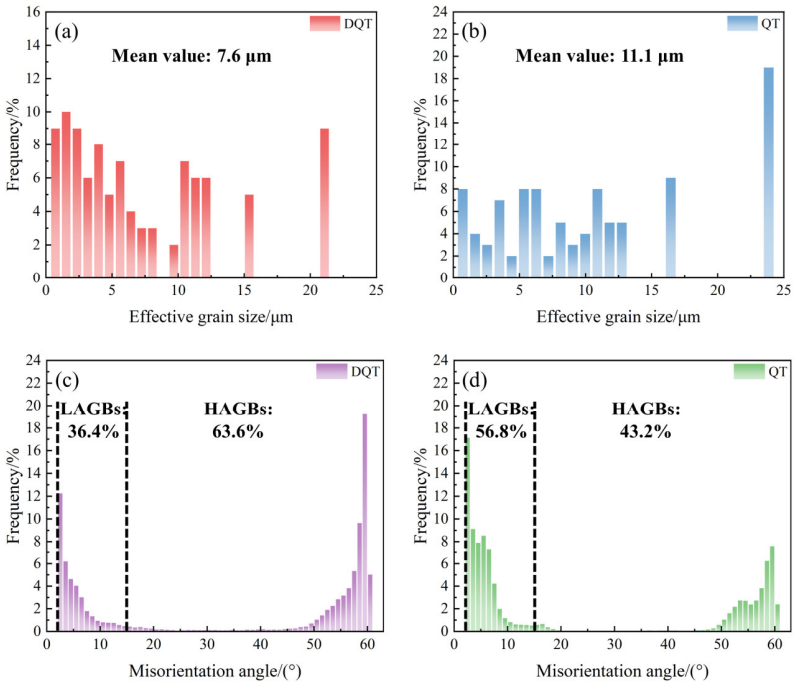


Figure 7. Grain size and grain boundary distributions of 0.025Nb steel under DQT and QT processes. Grain size distributions: (**a**) DQT, (**b**) QT; grain boundary distributions: (**c**) DQT, (**d**) QT.

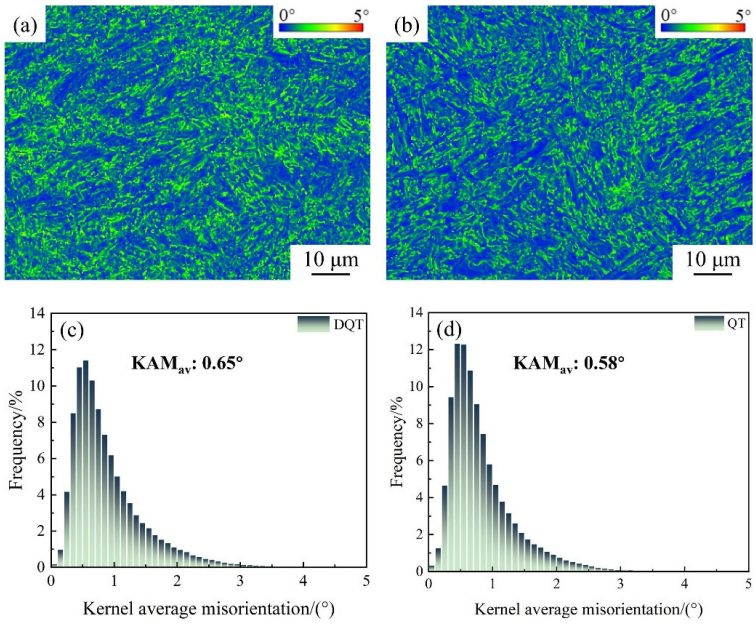


Figure 8. The KAM images of 0.025Nb steel under DQT and QT processes. DQT: (**a**,**c**). QT: (**b**,**d**).

3.4. The Effect of Nb Precipitation Behavior on Microstructural Evolution

Under the DQT process, rolling in the non-recrystallized zone introduced a large number of deformation bands and dislocations within the grain, increasing the deformation amount in the non-recrystallized zone and reducing the finishing rolling temperature, which was

conducive to increasing the dislocation substructure and deformation bands. This further refined the prior austenite grains and provided more nucleation sites for the precipitation of carbonitrides during cooling. In this experiment, the deformation amount of the non-recrystallized zone is close to 60%. The large deformation amount caused the formation of high-density dislocation walls, dislocation cells and deformation bands in the crystal, which limited the growth of martensite laths and played a role in refining the transformation products [42]. Due to direct quenching after rolling, there were two types of dislocations in the quenched martensite obtained. One type consisted of a large number of deformed dislocations formed during controlled rolling in the austenite region [43]. Due to strain induction, Nb, as a strong carbide-forming element, would precipitate a large amount of extremely fine carbonitrides between various passes of deformation, playing a pinning role in dislocations. When martensite transformation occurred, these dislocations would inherit some of the dislocations in the deformed austenite and remain pinned. Another kind of dislocation in laths was the transformation dislocation due to the volume effect during martensite transformation [44]. This kind of dislocation was relatively straight, and most of it was not pinned by precipitates, making it easy to disappear and rearrange during tempering.

Figure 9 shows the interaction between dislocations and precipitation in the DQT processes at different tempering temperatures. During the tempering process, there was a tendency for the microstructure to transition to a balanced structure. This transition inevitably involved the disappearance, recombination and reorganization of dislocations, and the speed of this process was determined by the mobility of dislocations. It can be seen that the martensite laths are thinner after direct quenching. After tempering at 450 °C, it is observed that network dislocations are pinned by a large number of fine dispersed precipitates. After tempering at 550 °C, the dislocation density is still high, and there is a dislocation wall formed by dislocation pileup. When the tempering temperature rises to 650 °C, the dislocation density decreases significantly, the M-A islands between laths decompose, and the precipitates coarsen.

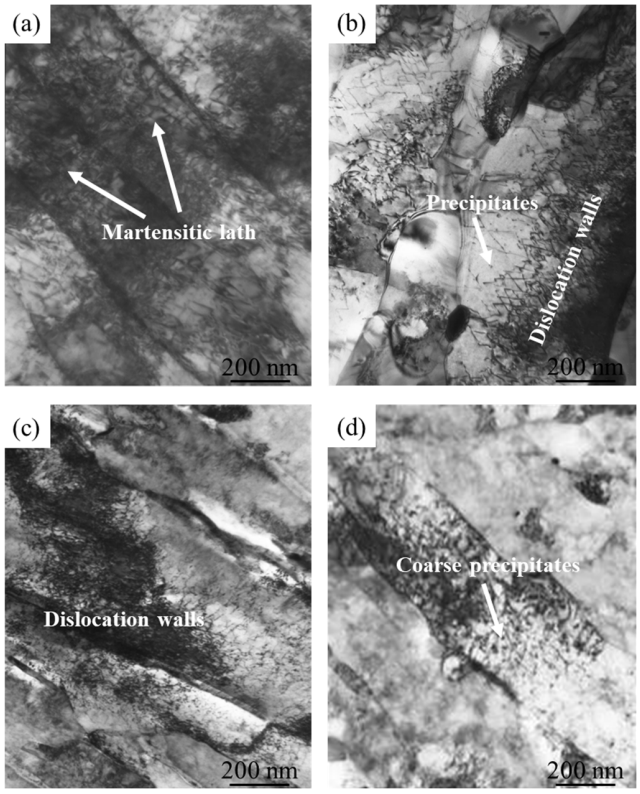


Figure 9. TEM images of microstructure evolution and precipitates at different tempering temperatures under the DQT process. (**a**) As-quenched; tempering at (**b**) 450 °C, (**c**) 550 °C, (**d**) 650 °C.

Figure 10e shows the energy spectrum analysis and selected area electron diffraction (SAED) of the precipitate, and determines that it is NbC. When tempered at 450 °C, the pinning effect of NbC precipitation on dislocations was strengthened, preferentially precipitating on dislocation lines, as shown in Figure 10a. The high dislocation density of martensite laths provided more precipitation nucleation sites, resulting in finer precipitation, more uniform distribution and a better strengthening effect, as shown in Figure 10b. As the tempering temperature increases, NbC gradually coarsens, the precipitation density decreases and the pinning effect decreases. At the same time, the increase in temperature also activates more movable dislocations, resulting in a decrease in yield strength, as shown in Figure 10c. When the tempering temperature rises to 650 °C, the NbC exhibits significant aggregation and spheroidization, as shown in Figure 10d. Besides reducing the pinning effect on dislocations, the blocking effect on the recovery process of deformed austenite is also relatively weakened, resulting in matrix softening. The increase in movable dislocations leads to a significant decrease in strength and an increase in ductility and toughness.

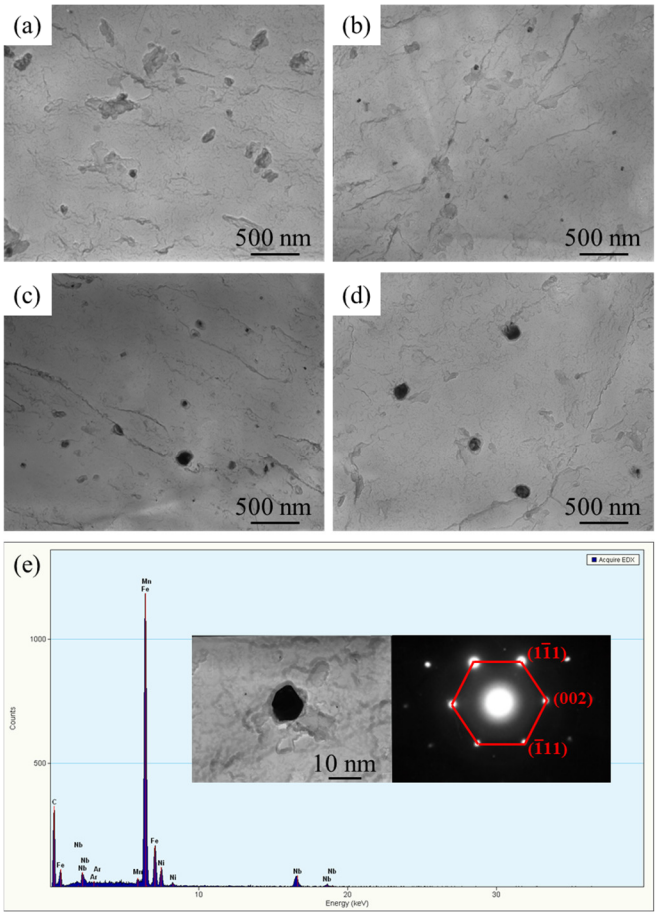


Figure 10. Micrographs and spectrum analysis of Nb precipitates under the DQT process. (**a**) As-quenched; tempering at (**b**) 450 °C, (**c**) 550 °C, (**d**) 650 °C; (**e**) energy spectrum analysis and SAED of precipitate.

According to Figure 11a, the quenched structure under the QT process is still typical lath-like martensite, with high dislocation density, and there are some retained austenite films between laths. After tempering at 450 °C, a large number of elongated acicular carbides with obvious orientation relationships appear in the microstructure of the QT process, as shown in Figure 11b. When the tempering temperature rises to 550 °C, the microstructure is significantly coarsened, and acicular carbides still exist, but the number is significantly reduced and in a dissolved state. The dislocation density further decreases, and is mainly deposited at the coarsened lath boundary, as shown in Figure 11c. When the

tempering temperature further rises to 650 °C, the lath-like structure can still be seen in the structure of the QT process. A large number of carbides are generated along the coarsened lath boundary, some of which have merged and grown. The dislocation distribution is disordered, but the presence of dislocations in place can still be observed, as shown in Figure 11d.

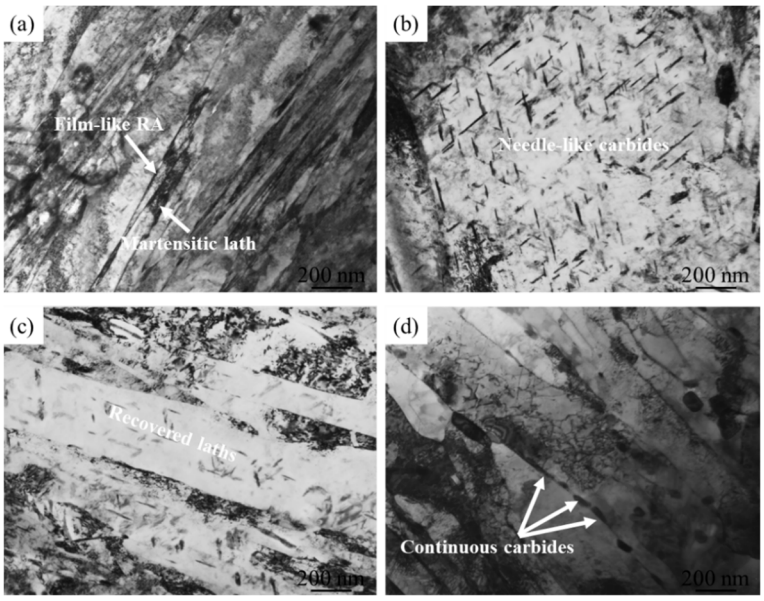


Figure 11. TEM images of microstructure evolution and precipitates at different tempering temperatures under the QT process. (**a**) As-quenched; tempering at (**b**) 450 °C, (**c**) 550 °C, (**d**) 650 °C.

4. Conclusions

In this study, the traditional off-line tempering heat-treatment process is replaced by the DQT process, which is effective in increasing production and reducing energy consumption and meets the requirements for use in the construction of large-scale pumped-storage power stations. The following specific conclusions can be drawn:

(1) Under the DQT process, a large number of deformation bands and dislocations were retained, and only the 0.025Nb DQT steel achieved cryogenic impact energy of more than 100 J at −60 °C, combined with the highest yield strength (986 MPa) and tensile strength (1037 MPa), owing to the highest total dislocation density of 1.8×10^{15} m^{-2}.

(2) The refining effect of the DQT process on martensite blocks and martensite laths increased the number and orientation of martensite block units, significantly increased the proportion of large angle grain boundaries, and thus promoted a significant increase in cryogenic impact toughness. The DQT process has a more obvious local strain concentration, mainly focusing on the refined lath boundary, which indicates that the refinement of microstructure also promotes the stacking of dislocations. The geometrically necessary dislocation density of 0.025Nb steel under the DQT and QT processes is 9.3×10^{14} m^{-2} and 8.3×10^{14} m^{-2}, respectively. The improvement in fine-grain strengthening and dislocation strengthening by the DQT process has jointly led to an increase in strength, resulting in a better combination of strength and toughness.

(3) Under the DQT process, the high dislocation density of martensite laths provides more precipitation nucleation sites, resulting in finer precipitation and more uniform distribution. As the tempering temperature increases, there are always high-density dislocation entanglements pinned by NbC, and NbC gradually coarsens. Under the QT process, when the tempering temperature increases, the microstructure is significantly coarsened, NbC merges and grows, and dislocation entanglement is significantly reduced.

Author Contributions: Conceptualization, H.W.; methodology, Z.P. and E.W.; software, E.W.; formal analysis, E.W.; writing—original draft preparation, Z.P. and E.W.; writing—review and editing, H.W. All authors have read and agreed to the published version of the manuscript.

Funding: This research was funded by the Key R&D Projects in Shandong Province (Major Scientific and Technological Innovation Projects), grant number 2023CXGC010310.

Data Availability Statement: The original contributions presented in the study are included in the article, further inquiries can be directed to the corresponding author.

Acknowledgments: The authors are particularly grateful for the support of CITIC Metal Co., Ltd.

Conflicts of Interest: Author Zhongde Pan was employed by the company Nanjing Iron and Steel Co., Ltd. The remaining authors declare that the research was conducted in the absence of any commercial or financial relationships that could be construed as a potential conflict of interest.

References

1. Zhao, Z.; Zhang, M.; He, M.; Gao, Y.; Li, J.; Han, S.; Liu, Z.; Lei, L.; Pérez Díaz, J.I.; Cavazzini, G.; et al. Beyond Fixed-Speed Pumped Storage: A Comprehensive Evaluation of Different Flexible Pumped Storage Technologies in Energy Systems. *J. Clean. Prod.* **2024**, *434*, 139994. [CrossRef]
2. Jia, T.; Wang, S.; Xiao, N.; Li, M. Quantitative Investigation on Strengthening and Toughening Mechanism of 1000 MPa Grade Hydropower Steel. *J. Mater. Eng. Perform.* **2023**, *32*, 2193–2204. [CrossRef]
3. Nikolaos, P.C.; Marios, F.; Dimitris, K. A Review of Pumped Hydro Storage Systems. *Energies* **2023**, *16*, 4516. [CrossRef]
4. Nations, U.; Griggs, D. Sustainable Development Goals for People and Planet. *Nature* **2015**, *495*, 305–307.
5. Chen, J.; Li, C.; Jin, X.; Chen, L.; Fang, L. Effect of Quenching Process on Microstructures and Mechanical Properties of Fe-0.9Mn-0.5Cr-2.4Ni-0.5Mo-C Steel. *J. Mater. Eng. Perform.* **2018**, *27*, 1505–1513. [CrossRef]
6. Hu, J.; Liu, K.K.; Ma, L.; Misra, R.D.K.; Zhang, W.N.; Du, H.C.; Xu, W. Significant Improvement in Strength and Toughness of Nanoscale Precipitate–Strengthened Steel by Direct Quenching and Tempering Process. *Steel Res. Int.* **2021**, *92*, 2000331. [CrossRef]
7. Xie, Z.J.; Shang, C.J.; Wang, X.L.; Ma, X.P.; Subramanian, S.V.; Misra, R.D.K. Microstructure-Property Relationship in a Low Carbon Nb-B Bearing Ultra-High Strength Steel by Direct-Quenching and Tempering. *Mater. Sci. Eng. A* **2018**, *727*, 200–207. [CrossRef]
8. Wu, B.B.; Wang, X.L.; Wang, Z.Q.; Zhao, J.X.; Jin, Y.H.; Wang, C.S.; Shang, C.J.; Misra, R.D.K. New Insights from Crystallography into the Effect of Refining Prior Austenite Grain Size on Transformation Phenomenon and Consequent Mechanical Properties of Ultra-High Strength Low Alloy Steel. *Mater. Sci. Eng. A* **2019**, *745*, 126–136. [CrossRef]
9. Wei, Y.; Li, Y.; Zhu, L.; Liu, Y.; Lei, X.; Wang, G.; Wu, Y.; Mi, Z.; Liu, J.; Wang, H.; et al. Evading the Strength-Ductility Trade-off Dilemma in Steel through Gradient Hierarchical Nanotwins. *Nat. Commun.* **2014**, *5*, 4580. [CrossRef]
10. Saastamoinen, A.; Kaijalainen, A.; Nyo, T.T.; Suikkanen, P.; Porter, D.; Kömi, J. Direct-Quenched and Tempered Low-C High-Strength Structural Steel: The Role of Chemical Composition on Microstructure and Mechanical Properties. *Mater. Sci. Eng. A* **2019**, *760*, 346–358. [CrossRef]
11. Hannula, J.; Kömi, J.; Porter, D.A.; Somani, M.C.; Kaijalainen, A.; Suikkanen, P.; Yang, J.R.; Tsai, S.P. Effect of Boron on the Strength and Toughness of Direct-Quenched Low-Carbon Niobium Bearing Ultra-High-Strength Martensitic Steel. *Metall. Mater. Trans. A* **2017**, *48*, 5344–5356. [CrossRef]
12. Wang, S.; Yu, H.; Zhou, T.; Wang, T. Effects of Non-Recrystallization Zone Reduction on Microstructure and Precipitation Behavior of a Ferrite-Bainite Dual Phase Steel. *Mater. Des.* **2015**, *88*, 847–853. [CrossRef]
13. Somani, M.C.; Porter, D.A.; Karjalainen, L.P.; Kantanen, P.K.; Kömi, J.I.; Misra, D.K. Static Recrystallization Characteristics and Kinetics of High-Silicon Steels for Direct Quenching and Partitioning. *Int. J. Mater. Res.* **2019**, *110*, 183–193. [CrossRef]
14. Krauss, G. Tempering of Lath Martensite in Low and Medium Carbon Steels: Assessment and Challenges. *Steel Res. Int.* **2017**, *88*, 1700038. [CrossRef]
15. Speer, J.; Matlock, D.K.; De Cooman, B.C.; Schroth, J.G. Carbon Partitioning into Austenite after Martensite Transformation. *Acta Mater.* **2003**, *51*, 2611–2622. [CrossRef]
16. Xu, Y.; Tan, X.; Yang, X.; Hu, Z.; Peng, F.; Wu, D.; Wang, G. Microstructure Evolution and Mechanical Properties of a Hot-Rolled Directly Quenched and Partitioned Steel Containing Proeutectoid Ferrite. *Mater. Sci. Eng. A* **2014**, *607*, 460–475. [CrossRef]
17. Ghosh, S.; Kaikkonen, P.; Javaheri, V.; Kaijalainen, A.; Miettunen, I.; Somani, M.; Kömi, J.; Pallaspuro, S. Design of Tough, Ductile Direct Quenched and Partitioned Advanced High-Strength Steel with Tailored Silicon Content. *J. Mater. Res. Technol.* **2022**, *17*, 1390–1407. [CrossRef]
18. Wu, Q.; He, S.; Hu, P.; Liu, Y.; Zhang, Z.; Fan, C.; Fan, R.; Zhong, N. Effect of Finish Rolling Temperature on Microstructure and Mechanical Properties of X80 Pipeline Steel by On-Line Quenching. *Mater. Sci. Eng. A* **2023**, *862*, 144496. [CrossRef]
19. Esterl, R.; Sonnleitner, M.; Gschöpf, B.; Schnitzer, R. Influence of V and Nb Micro-Alloying on Direct Quenched and Tempered Ultra-High Strength Steels. *Steel Res. Int.* **2019**, *90*, 1800640. [CrossRef]

20. Saastamoinen, A.; Kaijalainen, A.; Heikkala, J.; Porter, D.; Suikkanen, P. The Effect of Tempering Temperature on Microstructure, Mechanical Properties and Bendability of Direct-Quenched Low-Alloy Strip Steel. *Mater. Sci. Eng. A* **2018**, *730*, 284–294. [CrossRef]
21. Li, C.; Duan, R.; Fu, W.; Gao, H.; Wang, D.; Di, X. Improvement of Mechanical Properties for Low Carbon Ultra-High Strength Steel Strengthened by Cu-Rich Multistructured Precipitation via Modification to Bainite. *Mater. Sci. Eng. A* **2021**, *817*, 141337. [CrossRef]
22. Fu, W.; Li, C.; Di, X.; Fu, K.; Gao, H.; Fang, C.; Lou, S.; Wang, D. Refinement Mechanism of Nanoscale Cu-Rich Precipitates by Mo Addition and Its Effect on Strength-Toughness of Cu-Bearing Low Carbon High Strength Steel. *Mater. Sci. Eng. A* **2022**, *849*, 143469. [CrossRef]
23. Esterl, R.; Sonnleitner, M.; Schnitzer, R. Influences of Thermomechanical Treatment and Nb Micro-Alloying on the Hardenability of Ultra-High Strength Steels. *Metall. Mater. Trans. A Phys. Metall. Mater. Sci.* **2019**, *50*, 3238–3245. [CrossRef]
24. Takahashi, J.; Kawakami, K.; Hamada, J.I.; Kimura, K. Direct Observation of Niobium Segregation to Dislocations in Steel. *Acta Mater.* **2016**, *107*, 415–422. [CrossRef]
25. Tian, J.; Wang, H.; Zhu, M.; Zhou, M.; Zhang, Q.; Su, X.; Guo, A.; Xu, G. Improving Mechanical Properties in High-Carbon Pearlitic Steels by Replacing Partial V with Nb. *Mater. Sci. Eng. A* **2022**, *834*, 142622. [CrossRef]
26. Bai, B.H.; Shang, C.L.; Wu, H.H.; Ma, G.Q.; Wang, S.Z.; Wu, G.L.; Gao, J.H.; Chen, Y.M.; Zhang, J.Y.; Zhu, J.M.; et al. A review on the advance of low-temperature toughness in pipeline steels. *J. Mater. Res. Technol.* **2023**, *25*, 6949–6964. [CrossRef]
27. *ASTM E8*; Standard Test Methods for Tension Testing of Metallic Materials. American Society for Testing and Materials: Philadelphia, PA, USA, 2016.
28. Li, X.; Wiskel, J.B.; Henein, H.; Ivey, D.G.; Omotoso, O. Characterization of Microstructure in High Strength Microalloyed Steels Using Quantitative X-ray Diffraction. In Proceedings of the Biennial International Pipeline Conference, Calgary, AB, Canada, 29 September–3 October 2008; Volume 3, pp. 445–451.
29. Zhu, W.X.; Zhao, F.; Yin, S.; Liu, Y.; Yang, R.G. Effect of Tensile Deformation on Residual Stress of GH4169 Alloy. *Materials* **2021**, *14*, 1773. [CrossRef] [PubMed]
30. Antonov, S.; Chen, W.; Huo, J.; Feng, Q.; Isheim, D.; Seidman, D.N.; Sun, E.; Tin, S. MC Carbide Characterization in High Refractory Content Powder-Processed Ni-Based Superalloys. *Metall. Mater. Trans. A Phys. Metall. Mater. Sci.* **2018**, *49*, 2340–2351. [CrossRef]
31. Kim, D.W.; Kwon, D.Y.; Kang, J.H. Strengthening of High Nitrogen Austenitic Stainless Steel by Nb Addition. *Mater. Charact.* **2024**, *209*, 113776. [CrossRef]
32. Chen, J.; Ren, J.K.; Liu, Z.Y.; Wang, G.D. The Essential Role of Niobium in High Manganese Austenitic Steel for Application in Liquefied Natural Gas Tanks. *Mater. Sci. Eng. A* **2020**, *772*, 138733. [CrossRef]
33. Saastamoinen, A.; Kaijalainen, A.; Porter, D.; Suikkanen, P.; Yang, J.R.; Tsai, Y.T. The Effect of Finish Rolling Temperature and Tempering on the Microstructure, Mechanical Properties and Dislocation Density of Direct-Quenched Steel. *Mater. Charact.* **2018**, *139*, 1–10. [CrossRef]
34. Shukla, R.; Ghosh, S.K.; Chakrabarti, D.; Chatterjee, S. Microstructure, Texture, Property Relationship in Thermo-Mechanically Processed Ultra-Low Carbon Microalloyed Steel for Pipeline Application. *Mater. Sci. Eng. A* **2013**, *587*, 201–208. [CrossRef]
35. Lu, J.; Ni, L.; Wang, S.; Mao, X. Grey-Taguchi Analysis and Experimental Assessment of 1 GPa HSLA Steel Treated by Quenching and Tempering. *J. Mater. Res. Technol.* **2024**, *29*, 3508–3521. [CrossRef]
36. Tang, A.; Liu, H.; Chen, R.; Liu, G.; Lai, Q.; Zhong, Y.; Wang, L.; Wang, J.; Lu, Q.; Shen, Y. Mesoscopic Origin of Damage Nucleation in Dual-Phase Steels. *Int. J. Plast.* **2021**, *137*, 102920. [CrossRef]
37. Zhang, Y.; Wang, S.; Xu, G.T.; Wang, G.; Zhao, M.H. Effect of Microstructure on Fatigue-Crack Propagation of 18CrNiMo7-6 High-Strength Steel. *Int. J. Fatigue* **2022**, *163*, 107027. [CrossRef]
38. Xi, X.; Wu, T.; Wang, S.; Wang, J.; Wang, G.; Chen, L. Research on the Mechanism of Cu Addition on the Grain Boundary Characteristics and Toughness in CGHAZ of Low Carbon Low Alloy Steel. *J. Mater. Res. Technol.* **2023**, *23*, 577–586. [CrossRef]
39. Hayashi, T.; Morito, S.; Ohba, T. Local Distribution of Orientation Relationship and Microstructure Evolution of Lath Martensite in an Ultra-Low-Carbon Steel. *Scr. Mater.* **2020**, *180*, 1–5. [CrossRef]
40. Ressel, G.; Brandl, D.; Hönigmann, T.; Lukas, M.; Stark, A.; Gruber, C.; Lukas, S.; Stockinger, M.; Kozeschnik, E. Microstructural Refinement by Spontaneous Recrystallization without Prior Deformation of a 15–5 PH Steel Alloy and Its Mechanism. *Mater. Des.* **2023**, *234*, 112370. [CrossRef]
41. Zhang, Y.; Wu, H.; Yu, X.; Tang, D.; Yuan, R.; Sun, H. Microstructural Evolution and Strengthening Mechanisms in CrxMnFeNi High-Entropy Alloy. *J. Mater. Res. Technol.* **2021**, *12*, 2114–2127. [CrossRef]
42. Mao, W.; Gao, S.; Bai, Y.; Park, M.H.; Shibata, A.; Tsuji, N. Effective Grain Size Refinement of an Fe-24Ni-0.3C Metastable Austenitic Steel by a Modified Two-Step Cold Rolling and Annealing Process Utilizing the Deformation-Induced Martensitic Transformation and Its Reverse Transformation. *J. Mater. Res. Technol.* **2022**, *17*, 2690–2700. [CrossRef]

43. Dong, X.; Shin, Y.C. Predictive Modeling of Microstructure Evolution within Multi-Phase Steels during Rolling Processes. *Int. J. Mech. Sci.* **2019**, *150*, 576–583. [CrossRef]
44. Abou Ali Modad, O.; Shehadeh, M.A. Modeling Dislocation Interactions with Grain Boundaries in Lath Martensitic Steels. *J. Mater. Sci.* **2024**, *59*, 4829–4851. [CrossRef]

Disclaimer/Publisher's Note: The statements, opinions and data contained in all publications are solely those of the individual author(s) and contributor(s) and not of MDPI and/or the editor(s). MDPI and/or the editor(s) disclaim responsibility for any injury to people or property resulting from any ideas, methods, instructions or products referred to in the content.